Applying MICP Technology to Improve the Bond Strength of LWAC after High-Temperature Damage

How-Ji Chen , Yung-Hsiang Lo , Chao-Wei Tang * , Han-Wen Chang

Posted Date: 17 January 2024

doi: 10.20944/preprints202401.1291.v1

Keywords: biomineralization; high temperatures; fiber-reinforced lightweight aggregate concrete; bond strength

Article

Applying MICP Technology to Improve the Bond Strength of LWAC after High-Temperature Damage

How-Ji Chen [1], Yung-Hsiang Lo [1], Chao-Wei Tang [2,3,4,*] and Han-Wen Chang [1]

[1] Department of Civil Engineering, National Chung-Hsing University, 145 Xingda Rd., South District, Taichung City 40227, Taiwan; hojichen@dragon.nchu.edu.tw (H.-J.C.); sika.ericlo@gmail.com (Y.-H.L.); awiuyg58799@yahoo.com.tw (H.-W.C.)

[2] Department of Civil Engineering and Geomatics, Cheng Shiu University, No. 840, Chengching Rd., Niaosong District, Kaohsiung 83347, Taiwan

[3] Center for Environmental Toxin and Emerging-Contaminant Research, Cheng Shiu University, No. 840, Chengching Rd., Niaosong District, Kaohsiung 83347, Taiwan

[4] Super Micro Mass Research and Technology Center, Cheng Shiu University, No. 840, Chengching Rd., Niaosong District, Kaohsiung 83347, Taiwan

* Correspondence: tangcw@gcloud.csu.edu.tw; Tel.: +886-7-735-8800

Abstract: High temperatures can easily lead to a decline in the bond strength of reinforced concrete components. In view of this, this study utilized microbially induced calcium carbonate precipitation (MICP) technology to improve the bond strength of heat-damaged lightweight aggregate concrete (LWAC) after being exposed to 300 °C and 500 °C. The specimens of a control group (Group A) and two experimental groups (Group B and Group C) were prepared. These specimens healed themselves in different ways after exposure to high temperatures and a series of pull-out tests. Groups A and B adopted the same self-healing method, that is, placing their specimens in an incubator. Group C used different self-healing methods. The specimens in this group were soaked in a mixed solution of urea and calcium acetate for two days, and then taken out and placed in an incubator for two days. A self-healing cycle lasted four days until the desired age was reached. After being exposed to 300 °C and self-healed for 90 days, the relative bond strength ratio of Group C in the secondary pull-out test was the best. Compared with Group A, the relative bond strength ratio of Group C increased by 20.3%. This demonstrates that MICP technology could effectively improve the bond strength of LWAC after high-temperature and pull-out damage.

Keywords: MICP; heat damage; self-healing; pull-out test; bond–slip relationship

1. Introduction

Concrete mixed with lightweight aggregates (LWAs) instead of normal-weight aggregate is called lightweight aggregate concrete (LWAC). Since most LWAs are porous and have low specific gravity, LWAC is lightweight and has better seismic resistance than traditional normal-weight aggregate concrete (NWC) [1]. Taking structural LWAC as an example, its main benefit is to reduce the weight of the structure, so the size of columns, foundations, and other stress-bearing members can be reduced. Therefore, the inertial force generated by the earthquake due to the structure is relatively small, and the design load can be reduced to save on construction costs. Moreover, LWAC has very good thermal insulation performance, and its thermal conductivity is only half that of ordinary NWC. However, LWAC usually has higher levels of brittleness and worse mechanical properties compared with NWC, which has the same compressive strength [2]. With the advancement of science and technology, on the one hand, the production technology used for artificial lightweight aggregates (LWAs) has been continuously improved; on the other hand, nanosilica, nanoscale titanium oxide, and various fibers have been appropriately mixed into LWAC [3–6]. Therefore, fiber-reinforced LWAC with high strength and good toughness emerged as the times required, making its application in structural concrete more common [7–10].

 doi:10.20944/preprints202401.1291.v1

In reinforced concrete (RC) members, most researchers agree that the bond behavior between the rebars and the concrete mainly consists of three resistance mechanisms: adhesion, friction resistance, and rib support [11–17]. In terms of exploring the bond behavior between concrete and rebar, pull-out tests are generally used. Many studies have explored the bond behavior of rebars to LWAC at room temperature. Previously, the strength of LWAs was lower, resulting in LWAC having a worse bond strength than NWC at the same level of compressive strength [18]. However, some studies have shown the opposite result, namely, that LWAC has better bond strength. The research conducted by Mo et al. [19] showed that the peak bond stress of a well-confined LWAC could be expressed as $3.5\sqrt{f_c'}$. This is significantly larger than the value $2.5\sqrt{f_c'}$ suggested by the CEB-FIP standard [20]. Wang et al. [21] established a theoretical analysis model for the bond stress slip between rebars and LWAC. Liu et al. [22] studied the bond–slip characteristics between the corroded bars and LWAC. Yang et al. [23] proposed the bond–slip relationship of rebar in LWAC under the influence of additional embedded rebars around the central rebar. Tang [1] studied the bond–slip behavior of rebars embedded in LWAC. The results showed that the larger the rib height to the diameter ratio of the rebars, the greater the peak bond stress.

In contrast, there is relatively little research on the bond behavior between rebars and LWAC after being exposed to high temperatures. The failure of RC members exposed to fire mainly arises due to the reduction in the bond strength between the embedded rebars and concrete [24]. Kelvinley et al. [25] conducted experimental studies on the bond–slip behavior of rebars in fiber-reinforced LWAC at ambient and elevated temperatures, respectively. Their experimental results showed that exposure to high temperatures changed the failure mode from a more ductile pull-out mode to a brittle splitting mode. As a result, the peak bond strength and toughness of the specimen's bond-slip behavior were reduced. Tang [26] studied the effect of fiber blending methods on the bond strength of LWAC after exposure to high temperatures. His test results showed that the blending method of using one type of fiber or mixing two types of fiber had no significant effect on the residual bond strength of LWAC after being exposed to a temperature of 800 °C.

Due to many irresistible factors, RC members often exhibit cracks or local damage. If these cracks or local damage are not repaired in time or handled improperly, it will further lead to the loss of bond strength between rebars and concrete [27]. Therefore, repairing damaged concrete to extend the service life of RC structures has always been a research hotspot in the concrete academic community. General repairs use commercially available chemicals and polymers, which are sources of health and environmental risks [28]. In addition, these methods of repairing damaged concrete structures are less than satisfactory. In view of this, many researchers have changed their approach to biomineralization technology [29–33]. The use of insoluble compounds produced by microbial metabolism to fill cracks in concrete materials is a developing self-healing technology for concrete [34–36]. Therefore, research on microbially induced calcium carbonate precipitation (MICP) to repair concrete cracks is in the ascendant. However, if unprotected bacteria are added directly to concrete, which is highly alkaline in nature, it can easily lead to bacterial death. This results in a substantial reduction in bacterial populations [29]. Jones et al. [30] confirmed that alkali-resistant spore bacteria have the ability to repair cracks in concrete. To avoid the reduction in or disappearance of the bacterial population, appropriate carriers must be used to protect the bacteria [31]. Nimafar et al. [32] used bacteria to repair concrete cracks caused by high temperatures and improve concrete properties. Their test results showed an increase of 31–93% in the compressive strength of concrete specimens repaired with Saccharomyces pasteurianus and Bacillus sphaeroides. Chen et al. [33] used biomineralization technology to explore the self-healing properties of fiber-reinforced LWAC after its exposure to high temperatures. The test results showed that the bacterial mineralization in the experimental group was slow in the absence of an adequate source of nutrients. In addition, Chen et al. [9] applied biomineralization technology to improve damaged fiber-reinforced LWAC. Their test results showed that biomineralization technology could effectively improve the relative bond strength ratio of damaged fiber-reinforced LWAC.

The chemical composition, physical structure, and water vapor moisture content of LWAC change when it is exposed to high temperatures. This results in a severe decrease in its mechanical

 doi:10.20944/preprints202401.1291.v1

properties, which in turn affects the bond behavior between it and the rebars. We have identified few studies that explore the improvement of bond behavior between rebars and LWAC after exposure to high temperatures. In view of this, the purpose of this study is to apply MICP technology to improve the bond strength of fiber-reinforced LWAC after exposure to high temperatures. Fiber-reinforced LWAC specimens were prepared and sorted into a control group and two experimental groups; the former did not contain bacterial spores, and the latter two contained bacterial spores. For each group of specimens, the planned test items included a high-temperature test, a compressive strength test, and a series of pull-out tests. In addition, we also analyzed the precipitates formed at the cracks in the MICP-repaired specimens.

2. Materials and Methods

2.1. Experimental program

The novelty of this study is the application of MICP technology to improve the bond strength of LWAC after high temperatures and pull-out damage. Specimens for a control group (Group A) and two experimental groups (Group B and Group C) were prepared. The control group was mixed with LWAs that were not soaked in a bacterial solution or nutrient solution. The experimental group was mixed with LWAs soaked in a bacterial solution and a nutrient solution. When the concrete specimens had been cured to the age of 28 days, they were divided into two parts. A portion of the specimens was designed to undergo compressive strength and pull-out tests at room temperature. Another part of the specimen was first subjected to a high-temperature test. After reaching the target temperature and cooling to room temperature, the specimens were divided into unhealed ones and healed ones. The unhealed specimens were immediately subjected to the pull-out test. The healed specimens were first self-healed to the planned age, and then the pull-out test was performed. Groups A and B used the same self-healing method. placing their specimens in an incubator. Group C used different self-healing methods. The specimens in this group were soaked in a mixed solution of urea and calcium acetate for two days, and then taken out and placed in an incubator for two days. A self-healing cycle lasted four days until the desired age was reached. After self-healing, the damaged specimens were subjected to a secondary pull-out test. Table 1 lists the test items and test parameters of this study. The test project is mainly a series of pull-out tests. The test parameters include the self-healing method, self-healing age, and target temperature.

Table 1. Test items and test parameters.

Test Items	Test Parameters		
	Curing/healing method	Self-healing age (day)	Target temperature (°C)
Pull-out test (before and after exposure to high temperatures)	Incubator, water tank	0, 28, 90	300, 500
Secondary pull-out test (after self-healing)	Incubator and cyclical treatment	28, 90	300, 500
Observation of crack repair of the pull-out specimens after exposure to high temperatures	Incubator and cyclical treatment	7, 14, 21, 28	300, 500
FESEM, EDS, and XRD analyses	Incubator and cyclical treatment	0, 28	300, 500

2.2. Materials

The materials used in this research are divided into a bacteria culture and a concrete composition. In terms of the bacterial culture, the materials used include *Sporosarcina pasteurii* (*S. pasteurii*), calcium lactate, yeast extract, calcium acetate, and urea. *S. pasteurii* is a gram-positive bacterium. It is capable of precipitating calcite in the presence of a calcium source and urea. Calcium

Preprints (www.preprints.org) | NOT PEER-REVIEWED | Posted: 17 January 2024 doi:10.20944/preprints202401.1291.v1

lactate is a milky-white compound formed by the combination of lactic acid bacteria and calcium. It served as a nutrient source for *S. pasteurii*. Yeast extract is the concentrated content of yeast cells. Its solution, mixed with calcium lactate, was used as a source of nutrients for *S. pasteurii*. Calcium acetate was used as a supplementary source of external calcium ions during the maintenance of the specimens. Urea is an organic compound composed of carbon, nitrogen, oxygen, and hydrogen. It was used as a source of carbonate ions for MICP during the self-healing process of LWAC.

For the concrete testing, the materials used include cement, water, fine aggregate, lightweight coarse aggregate, superplasticizer, fiber, reinforcement, and thermocouple. The cement was a locally produced Type I Portland cement with a specific gravity of 3.15 and a fineness of 3550 cm^2/g. The water was normal tap water, which is in line with the general quality requirements of concrete mixing water. The fine aggregate was a natural river sand with an FM value of 2.7 and a 24-hour water absorption rate of 1.15%. The LWA was an expanded shale artificial aggregate (as shown in Figure 1) with a dry unit weight of 618.8 kg/m^3, an apparent gravity of 1.23, and a crushing strength of 4.4 MPa.

Figure 1. Appearance of expanded shale LWAs.

The superplasticizer complies with the requirements of Type F of ASTM C494/C494M-17 specifications. The fibers included steel fibers and polypropylene fibers. The length, diameter, density, elastic modulus, and tensile strength of the steel fibers were 13 mm, 0.2 mm, 7.8 g/cm^3, 200 GPa, and 2000 MPa, respectively. The length, diameter, density, tensile strength, and melting point of the polypropylene fibers were 12 mm, 0.05 mm, 0.9 g/cm^3, 300 MPa, and 165 °C, respectively. The reinforcement was #6 rebar that used for the longitudinal main reinforcement of the pull-out. Its nominal diameter, rib distance, rib width, rib height, yield strength, and tensile strength are 19.1 mm, 11.1 mm, 4.0 mm, 1.0mm, 457 MPa, and 658 MPa, respectively. The thermocouple was a K-type nickel–aluminum alloy, with a sensitivity of 41 μV/°Cand a temperature range of -50 °C to 1200 °C.

2.3. Strain implantation and the Mixing Proportions of LWAC

For the culture of bacterial strains and sporulation, refer to the author's previously published article [37]. The LWAC specimens of the control group (Group A) and the experimental groups (Group B and Group C) were made. The LWAs used in Group A were not implanted with bacterial strains, while the LWAs used in Groups B and C were implanted with bacterial strains. Detailed steps for implanting bacterial strains into LWAs can be found in the author's previously published article [9]. The required 28-day compressive strength of each group of LWAC was 45 MPa. Considering the fresh and hardened properties of the LWAC, the amount of each material was determined through trial mixing. Each group of LWAC had the same mix proportions, as shown in Table 2. The mixing of each group of concrete followed ASTM C511 specifications.

Table 2. Mix proportions of the concretes.

W/B	Water (kg/m^3)	Cement (kg/m^3)	LWA (kg/m^3)	FA (kg/m^3)	SF (kg/m^3)	PP (kg/m^3)	SP (kg/m^3)
0.45	220	489	345	734	58.5	1.17	0.978

Notes: W/B: water–binder ratio; LWA: lightweight aggregate; FA: fine aggregate; SF: steel fiber; PP: polypropylene fiber; SP: superplasticizer.

Preprints (www.preprints.org) | NOT PEER-REVIEWED | Posted: 17 January 2024 doi:10.20944/preprints202401.1291.v1

2.4. The casting and curing of the specimens

For the compression test, we used a cylindrical specimen with a diameter of 100 mm and a height of 200 mm. The pull-out specimen was a cube with a side of 150 mm, and a #6 rebar was embedded vertically along its central axis, as shown in Figure 2. The embedded length (l_e) was three times the rebar diameter (d_b) to create a local bonding. In order to achieve the effect of local bonding, the unbounded regions of the rebars were wrapped with PVC sleeves when casting the pull-out specimens. In addition, to prevent the rebars of the specimens from being corroded during the curing process, the joints between the PVC sleeves and the rebars were filled with water-based sealant, and high-temperature anti-rust paint was sprayed on the surface of the protruding rebars. Moreover, the specimen contained three transverse stirrups to prevent its splitting failure when the rebar was under tension.

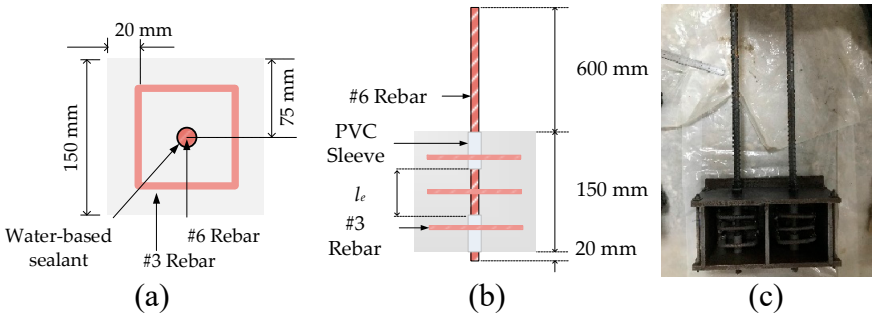

Figure 2. Dimensions and cross-sections of the pull-out specimens: (a) top view; (b) side view; and (c) photo of the specimen mold.

After the mixing operation of each group of concrete mixtures was completed, the slump was measured and recorded. Then, according to the relevant regulations of the ASTM, twenty-four cylindrical specimens and thirty-six pull-out specimens were cast for each group of concrete mixtures. The specimens were demolded after 24 hours. All specimens were then placed into a saturated limewater tank in a curing room. On the 14th day, the specimens were taken out and placed in a 40 °C incubator for 14 days. After casting and curing for 28 days, compressive strength, high-temperature, and pull-out tests were conducted on each group of specimens. Then, different self-healing methods were used for each group of specimens damaged in the high-temperature and pull-out tests.

2.5. Test methods and data analysis

The concrete slump was carried out in accordance with ASTM C143. The concrete unit weight was determined in accordance with ASTM C138. The cylindrical specimens were tested for their compressive strengths according to ASTM C39 and for their static modulus of elasticity according to ASTM C469. The compressive strength and static modulus of elasticity were the average values of three specimens. The pull-out test was carried out following the specifications of ASTM C234. A 200 kN MTS servo valve-controlled machine equipped with a special test frame was used to apply the tensile force to the pull-out specimen, as shown in Figure 3.

Preprints (www.preprints.org) | NOT PEER-REVIEWED | Posted: 17 January 2024 doi:10.20944/preprints202401.1291.v1

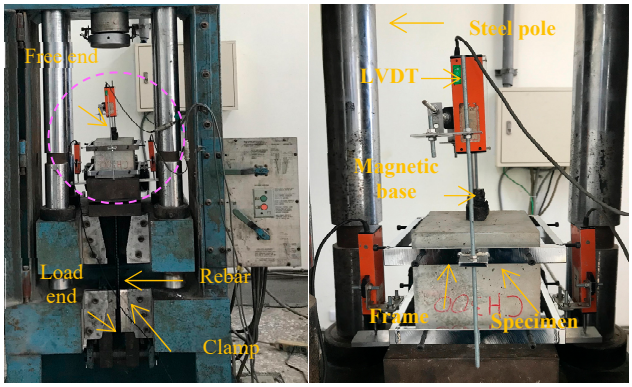

(a) (b)

Figure 3. Setup of the pull-out test: (a) overall configuration; (b) local configuration. .

The embedded rebar of the pull-out specimen was loaded at one end and was set to a free state at the other end, as shown in Figure 3a. Three linear variable differential transformers (LVDT) were set up using the test frame to measure the relative bond slip between the rebar and concrete at the load end and free end, as shown in Figure 3b. The transmission lines of the load and LVDT were connected to the data acquisition device, and the test started after zeroing. The load was applied at a constant displacement rate of 0.01 mm/s throughout the test until specimen failure.

Referring to the literature [38], assuming that the bond stress is uniformly distributed along the length of the rebar, the bond stress is calculated as follows:

$$\tau = \frac{P}{\pi d_b l_e} \tag{1}$$

where τ= the bond stress; P = the applied load; d_b= the rebar diameter; and l_e = the embedded length.

After the specimens were cured for 28 days, the incubator was adjusted to 60 °C for five days to dry the moisture inside the concrete specimens, to reduce the risk of the specimens spalling at high temperatures. To understand the relationship between the temperature of the concrete inside the pull-out specimen and the heating time, thermocouples were embedded at different places inside the specimen. Two thermocouples were embedded in the 150-mm cubic concrete block of the pull-out specimen, one 2 cm away from the surface of the specimen and the other 4 cm away (as shown in Figure 4).

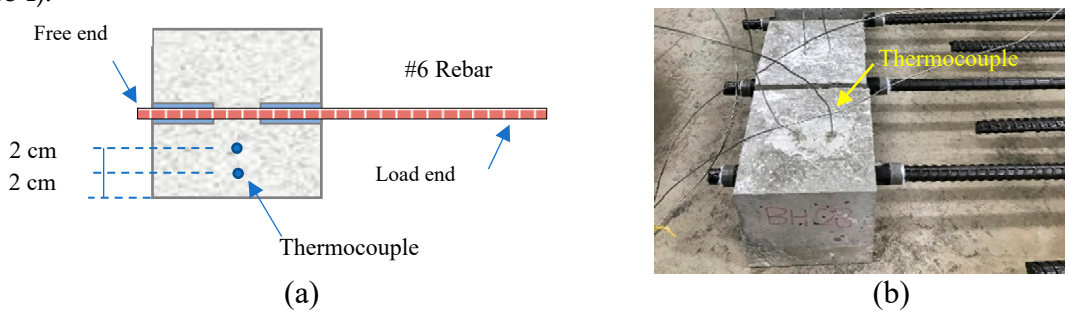

(a) (b)

Figure 4. Thermocouple for the pull-out test specimen: (a) schematic diagram of the location of the thermocouple; (b) actual pull-out specimens.

During the high-temperature test, the heating rate of the specimen was 10 °C/min. After the target temperature was reached, the power supply of the high-temperature furnace was turned off immediately. After the specimens were naturally cooled to room temperature in the high-temperature furnace, the residual bond strength was tested. According to the different states of the specimens, the pull-out test of LWAC was divided into five types. The test sequences for these five types of pull-out tests are shown in Table 3.

Preprints (www.preprints.org) | NOT PEER-REVIEWED | Posted: 17 January 2024 doi:10.20944/preprints202401.1291.v1

Table 3. Pull-out test items and test sequence.

Test Item	Test Sequence
Pull-out test of the LWAC after 28 days of curing at room temperature	Curing→loading
First pull-out test of the unhealed LWAC damaged in high-temperature tests	Curing→heating→loading
Secondary pull-out test of the unhealed LWAC damaged in high-temperature and first pull-out tests	Curing→heating→loading→self-healing→reloading
First pull-out test of the healed LWAC damaged in high-temperature tests	Curing→heating→self-healing→loading
Secondary pull-out test of the healed LWAC damaged in high-temperature and first pull-out tests	Curing→heating→self-healing→loading→self-healing→reloading

Furthermore, FESEM and EDS were used to observe and analyze the microstructure of each group of concrete samples that were self-repaired after being exposed to high temperatures. The purpose of this process is to examine the formation of hydration products and their morphology. Using the concrete cylindrical specimens that were damaged after the compression test, samples were taken from two different parts of the cylindrical specimens in each group of LWAC specimens, that is, two centimeters closer to the surface and the center for FESEM observation. Before performing FESEM and EDS, the sample must be in a dry state to facilitate the subsequent operations. The selected fragments were first cleaned, dried, and gilded. Afterward, scanning electron microscopy observations were undertaken to understand the micro-structural characteristics and differences of each group of concrete. Furthermore, in order to understand the element types and contents of each group of concrete samples, XRD analysis was used to conduct qualitative and semi-quantitative analyses. In other words, FESEM, EDS, and XRD were used to analyze the reasons why concrete samples with different self-healing methods show different residual properties after high-temperature exposure.

3. Experimental Results and Discussions

3.1. Results of the Fresh Properties Test and Compression Test

The slump test results show that each mixture had appropriate workability, with a slump value of 13 cm. At the same time, the unit weight of each mixture was 1849 kg/m^3 (20% less than ordinary NWC), which met the requirements of general LWAC. Figure 5 shows the 28-day compressive strength test results of each group of LWAC at room temperature. As shown in Figure 5, the 28-day compressive strength of each group was similar to the required 28-day compressive strength. Overall, the structural efficiency (strength/density) of each group was 24.3 MPa/(t/m^3). This value was already within the structural efficiency range of most LWACs, that is, 10-40 MPa/(t/m^3) [39]. On the other hand, the 28-day elastic modulus of each group was also almost the same, ranging from 18.75 to 19.26 GPa. For a typical expanded clay-LWA-cast LWAC, its elastic modulus is generally in the range of 10–20 GPa. Therefore, these results are consistent with the literature [40,41].

Preprints (www.preprints.org) | NOT PEER-REVIEWED | Posted: 17 January 2024 doi:10.20944/preprints202401.1291.v1

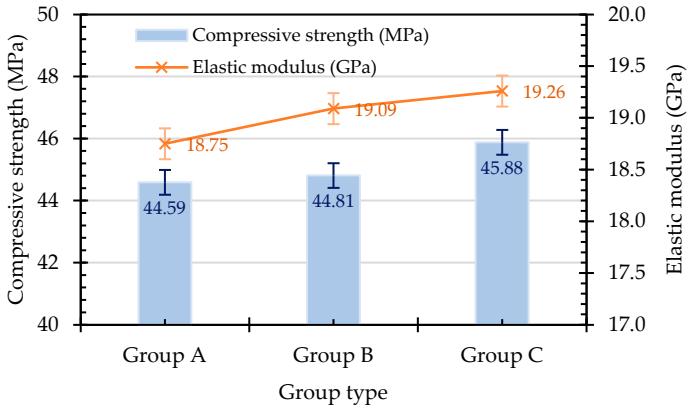

Figure 5. Compressive strength and elastic modulus of LWAC.

3.2. Results of the Pull-Out Test

3.2.1. Local Bond–Slip Relationship and Bond Strength in LWAC at Room Temperature

Under room-temperature conditions, the failure modes of the specimens in each group showed rebar pull-out failure. One characteristic of this phenomenon is that the longitudinal rebar of the specimen was pulled out of the concrete, while only a few cracks appeared in the surrounding concrete. In other words, no splitting failure occurred in the specimen during the pull-out test process. This can be attributed to the presence of stirrups, which effectively confined the specimen and limited the development of cracks. In this study, the concrete cover of the pull-out specimens was relatively thick (6.5 cm) and surrounded by transverse stirrups. Therefore, the longitudinal rebar of the specimen was subject to greater confinement. The concrete between the transverse ribs was sheared off due to punching, causing the rebar to be pulled out of the concrete directly. Generally, the concrete cover-to-diameter of the rebar (C/D) ratio is in the range of 2.5–3.0, which can ensure that the failure mode is rebar pull-out failure [42]. The C/D ratio of the pull-out specimen in this study was 3.4; thus, all the pull-out specimens suffered rebar pull-out failure.

Literature data shows that the rebar slipping at the end of the peak bond stress of the pull-out specimen is roughly in the range of 2–6 mm [20,43]. In view of this, the first pull-out test of the specimen was terminated when the rebar slippage reached 5 mm. Then, the damaged specimens were allowed to heal themselves in a planned manner before conducting a secondary pullout test. Therefore, the analysis of the first pull-out test of each group of specimens only focused on the slip of the rebar in the range of 0–5 mm. The local bond stress–slip (τ–s) relationship curves of the pull-out tests for each group of specimens at room temperature are shown in Figure 6.

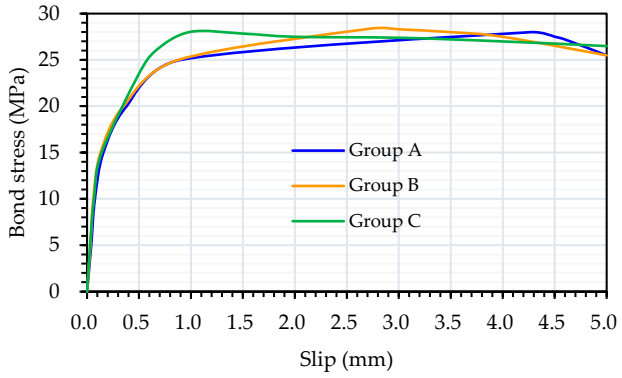

Figure 6. Local bond stress–slip relationship curve of each group of specimens at room temperature.

As shown in Figure 6, with the increase in load, the curves of each group of specimens in the pull-out test could be divided into linear ascending, nonlinear ascending, and descending stages. It is worth noting that the ascending branch of the τ–s relationship of LWAC exhibited a more linear relationship. This is attributed to the better chemical adhesion and greater tensile strength of the

Preprints (www.preprints.org) | NOT PEER-REVIEWED | Posted: 17 January 2024 doi:10.20944/preprints202401.1291.v1

cement matrix of LWAC. This is consistent with Tang's research results [38]. The surfaces of the specimens that suffered pull-out failure exhibited neither any splitting cracks nor any sudden drop in bond stress when it reached its peak. In addition, the peak bond stress of Group B and Group C was slightly higher than that of Group A, but the corresponding slip to the peak bond stress was smaller, and its value was about 1–3 mm.

The bond strength of the pull-out specimens was analyzed based on the experimental data captured during the pull-out tests. Figure 7 shows the bond strength of the first pull-out test for each group of specimens. As shown in Figure 7, at room temperature, the average bond strengths of each group at the age of 28 days were close to 28 MPa. These bond strength values significantly exceeded the values recommended by Mo et al. [19] ($3.5\sqrt{f_c'}$) and the CEB-FIP standard ($2.5\sqrt{f_c'}$) [20]. This result is consistent with the results of Kevinly et al. [25]. This is due to the stronger aggregate interlocking effects of the LWAs and the higher content of cementitious materials in LWAC, which improved the quality of the cement paste. As a result, the mechanical interlocking performance of the LWAC improved [19,23].

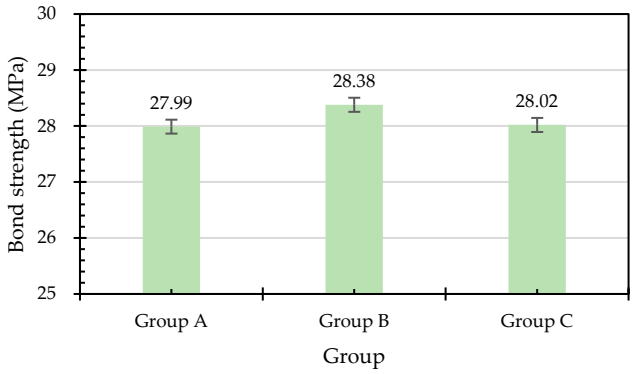

Figure 7. Bond strength of LWAC at room temperature.

3.2.2. Local Bond–Slip Relationship and Bond Strength in Unhealed LWAC after Exposure to High Temperatures

The high-temperature test was carried out immediately after casting and curing each group of specimens for 28 days. The high temperature test used a faster heating rate, that is, 10 °C/min. Once the high-temperature furnace reached the target temperature, the power was turned off. After exposure to 300 °C and 500 °C, there was no obvious spalling of the two groups of LWAC specimens. Theoretically, a longer embedded length of rebars will lead to strain penetration [44], which makes the strain distribution of the rebars along the longitudinal direction uneven, resulting in lower bond strength in the concrete. In the pull-out test, the bond anchorage length of the rebar was set to be short (l_e=3d_b). Therefore, the rebar essentially remains in the elastic stage [45]. As mentioned above, for rebars with short bonded anchor lengths, good restraint, and adequate cover, the pull-out specimen should exhibit rebar pull-out failure. After being exposed to high temperatures, concrete specimens suffered some degree of heat damage. The pull-out test results of both the control group and the experimental group showed rebar pull-out failure.

As mentioned previously, thermocouples were embedded inside the pull-out specimens, 2 and 4 cm away from the surface of the specimen (as shown in Figure 4). Under the condition of a target temperature of 300 °C, the maximum temperatures at 2 and 4 cm from the surface of the concrete specimen were about 98.2 °C and 90.8 °C, respectively, as shown in Figure 8a. Under the condition of a target temperature of 500 °C, the maximum temperatures at 2 and 4 cm from the surface of the concrete specimen were about 235.7 °C and 230 °C, respectively, as shown in Figure 8b. From this point of view, the temperature difference between these two places inside the concrete was about 5.7–7.4 °C. In addition, even though the target temperature was 500 °C, the maximum temperature inside the specimen did not yet reach 240 °C. Metha and Monteiro [46] pointed out that when the heating temperature of concrete reaches above 200 °C, cement hydrates gradually decompose and aggregates decay. For example, calcium silicate (C-S-H) colloids begin to lose bonding water and

Preprints (www.preprints.org) | NOT PEER-REVIEWED | Posted: 17 January 2024 doi:10.20944/preprints202401.1291.v1

undergo chemical changes. However, the internal temperature of the concrete specimen did not exceed 250 °C, and the changes in its microstructure and properties were still slight. In other words, the high temperature test did not cause significant degradation of the matrix of the concrete specimens in each group.

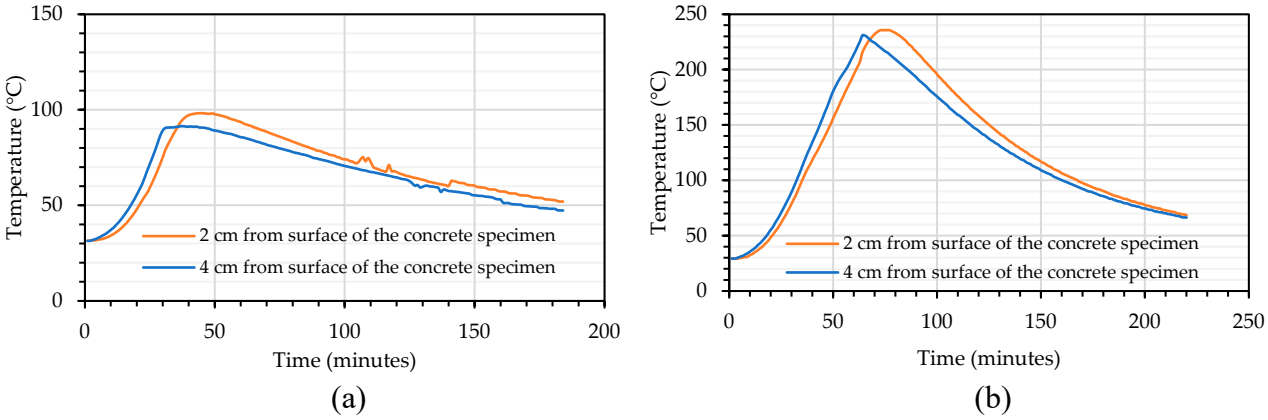

Figure 8. Relationship curve between the temperature of the concrete and time inside the pull-out specimen: (a) target temperature 300 °C; (b) target temperature 300 °C.

The τ–s relationship curves of the unhealed specimens after exposure to high temperatures are shown in Figure 9. As shown in Figure 9, the τ–s relationship curves of the LWAC specimens after exposure to high temperatures could be divided into different stages, that is, linear ascending, non-linear ascending, and descending stages. Regardless of whether the target temperature was 300 °C or 500 °C, there was no significant difference in the peak bond stress between the experimental group and the control group, and the corresponding slip to the peak bond stress was between 1 and 3 mm.

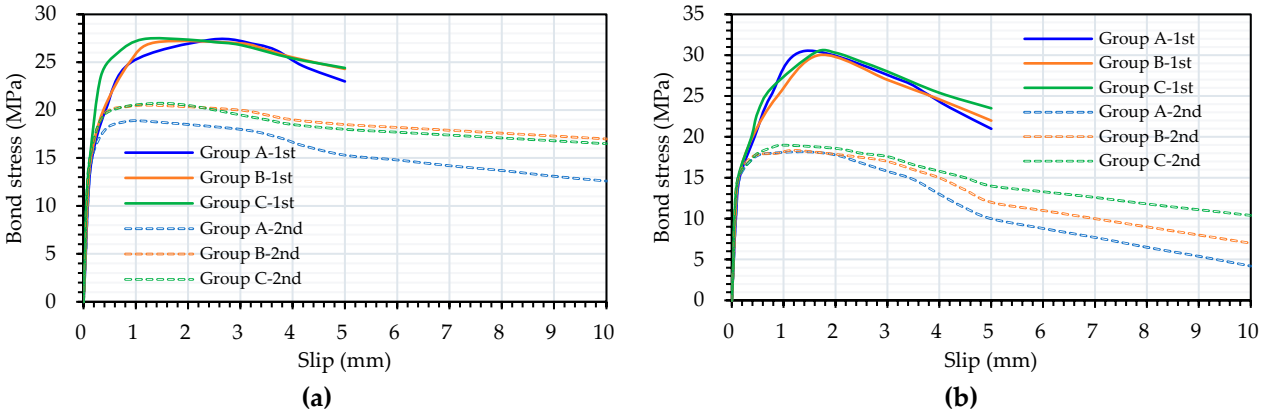

Figure 9. Local bond stress–slip relationship curves of unhealed LWAC specimens after exposure to high temperatures: (a) at a target temperature of 300 °C; (b) at a target temperature of 500 °C.

On the other hand, each group of specimens that experienced rebar pull-out failure healed themselves according to the planned self-healing method. Once these specimens healed themselves to the planned age, a secondary pull-out test was performed. During the secondary pull-out test, the test was stopped only when the specimen failed completely. That is, the rebar slippage was not limited to 5 mm. Taking each group of specimens exposed to 300 °C as an example, an obvious plateau appeared in the τ–s relationship curve, as shown in Figure 9a. At this stage, the bond stress decreased slowly, but the slip continued to increase. Then, the bond stress decreased significantly. Overall, the bond-slip curve of each group of LWAC specimens was consistent with the model suggested by CEB-FIP 2000 [20]. In other words, it could be divided into four stages: linear ascending, non-linear ascending, descending, and residual stages. In the linear ascending branch, the specimen had no obvious cracks and was in an elastic state. In the non-linear ascending branch, the cracks in the specimen expanded and were in a continuous cracking state. In the descending branch, the specimen was completely cracked and was penetrated by cracks. In the residual branch, the bond

Preprints (www.preprints.org) | NOT PEER-REVIEWED | Posted: 17 January 2024 doi:10.20944/preprints202401.1291.v1

stress of the specimen was mainly composed of pure friction resistance. Moreover, after exposure to 300 °C, Figure 9a shows that the peak bond stress of the secondary pull-out test in the experimental group was significantly higher than that in Group A. However, after exposure to 500 °C, Figure 9b shows that there was no significant difference in the peak bond stress of the secondary pull-out test between the experimental group and the control group.

The τ–s relationship curves of the control group and the experimental group after being exposed to different temperatures without healing are shown in Figures 10 and 11, respectively. Figures 10 and 11 indicate that, as the target temperature increased, the slope of the linear ascending branch in the figures tended to become steeper. The load of each group was the largest after being exposed to a temperature of 500 °C, followed by room temperature and 300 °C. Compared with room-temperature conditions, the maximum load of each group of specimens after being subjected to 500 °C increased by about 6% to 9%. Regarding the plateau sections of each group shown in Figures 10 and 11, the experimental group had a smaller attenuation range after entering the plateau section than Group A. This strength attenuation rate increased with the increase in the target temperature, and it can be seen that the specimens subjected to temperatures of 500 °C were particularly obvious. As shown in Figure 10, when the target temperature was 300 °C, the peak bond stress of the Group A specimens decayed only slightly. When the target temperature was 500 °C, the peak bond stress of Group A showed a phenomenon of increasing instead of decreasing. Moreover, after being subjected to different temperatures, there was no significant difference in the peak bond stress of the secondary pull-out test in Group A.

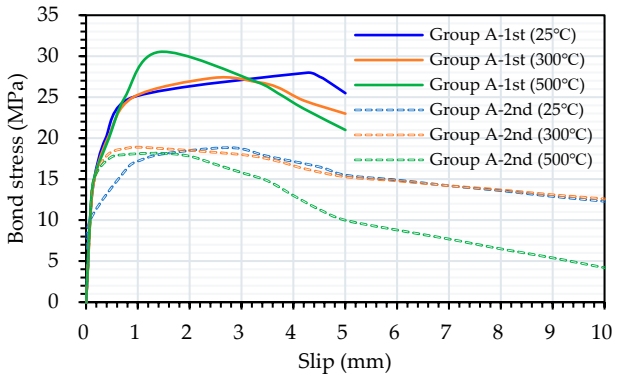

Figure 10. Local bond stress–slip relationship curves of unhealed Group A specimens after exposure to different temperatures.

Under the conditions of different temperatures, the τ–s relationship curve of the experimental group is shown in Figure 11. As shown in Figure 11a, when the target temperature was 300 °C, the peak bond stress of the specimens in Group B decayed only slightly. When the target temperature was 500 °C, the peak bond stress of the Group B specimens showed a phenomenon of increasing instead of decreasing. In addition, after being subjected to different temperatures, the peak bond stress of the secondary pull-out test of Group B was significantly different. When the target temperature was 500 °C, the peak bond stress of the specimen decreased sharply. Furthermore, as shown in Figure 11b, when the target temperature was 300 °C, the peak bond stress of the Group C specimens decayed only slightly. When the target temperature was 500 °C, the peak bond stress of the Group C specimens did not decrease but instead increased. In addition, after being subjected to different temperatures, the peak bond stress of the secondary pull-out test of Group C was significantly different. That is, the higher the target temperature, the smaller the limit of the bond stress. Furthermore, compared with the control group, the slope in the linear ascending branch of the experimental group was higher and became steeper as the target temperature increased, as shown in Figures 10 and 11. Observing the slip growth trend after 3 mm, at room temperature and 300 °C, the curve of the experimental group tended to be flat and slightly attenuated, while the curve of Group A exhibited an obvious downward trend.

Preprints (www.preprints.org) | NOT PEER-REVIEWED | Posted: 17 January 2024 doi:10.20944/preprints202401.1291.v1

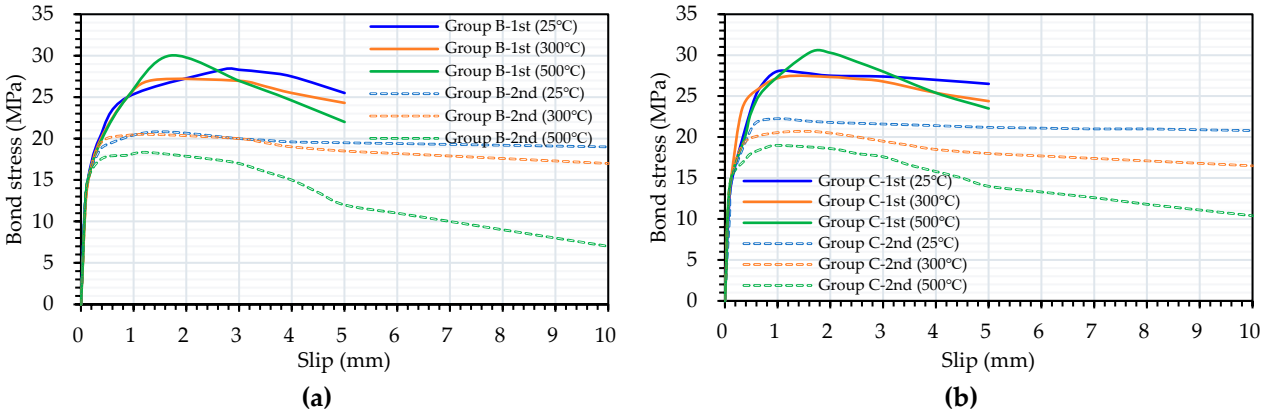

Figure 11. Local bond stress–slip relationship curves of unhealed experimental group specimens after exposure to different temperatures: (a) Group B; (b) Group C.

The results of the first pull-out test of each group after the high-temperature test and without self-healing are shown in Table 4. When the maximum target temperature was 300 °C, the maximum concrete temperature inside the pull-out specimen was about 98.2 °C. Therefore, the internal temperature of the specimen did not cause the concrete substrate to decay, so its residual bond strength did not decrease significantly. Table 4 shows that, after exposure to 300 °C, the average bond strength of the unhealed specimen in each group was close to 27 MPa. These bond strength values were only slightly lower than the bond strengths of each group of specimens at room temperature. After being subjected to 500 °C, the average first bond strength of the unhealed specimens in each group was close to 30 MPa. These bond strength values were higher than those of each group of specimens at room temperature. When the maximum target temperature was 500 °C, the maximum concrete temperature inside the pull-out specimen was about 235.7 °C. The bond strength of the specimen was slightly increased due to the drying effect caused by the high-temperature evaporation of water vapor inside the specimens [47]. On the other hand, based on the bond strength of the specimen at room temperature, the residual bond strength after the high temperatures was divided by the bond strength at room temperature, and the relative bond strength ratio was calculated as shown in Table 4. As shown in Table 4, the relative bond strength ratios of Group A, Group B, and Group C after exposure to high temperatures were between 0.98 and 1.09, 0.95 and 1.06, and 0.98 and 1.08, respectively.

Table 4. Bond strength of unhealed LWAC after exposure to high temperatures.

Group	BS at RT (MPa)	Residual BS (MPa)		Relative BS Ratio	
		300 °C	500 °C	300 °C	500 °C
Group A	27.99 (1.56)	27.35 (0.68)	30.53 (1.75)	0.98	1.09
Group B	28.38 (1.34)	27.07 (1.14)	30.02 (1.97)	0.95	1.06
Group C	28.02 (0.40)	27.41 (0.69)	30.34 (1.20)	0.98	1.08

Note: BS: bond strength; RT: room temperature; the data in brackets are standard deviations.

In addition, each group of specimens that were damaged by the high temperatures and pull-out tests were healed. The results of the secondary pull-out test after 28 days of self-healing are shown in Table 5. It can be seen that, when the target temperature was 300 °C, the residual bond strengths of the secondary pull-out test results of Group A, Group B, and Group C were 18.89, 20.48, and 20.70 MPa, respectively. Compared with the specimens in Group A, the relative bond strength ratios of the specimens in Group B and Group C after 28 days of self-healing increased by 5.9% and 8.8%, respectively. However, as the target temperature reached 500 °C, the residual bond strengths of the secondary pull-out test results of Group A, Group B, and Group C were 18.17, 18.35, and 19.00 MPa, respectively. As shown in Table 5, the relative bond strength ratios of Group A, Group B, and Group C in the secondary pull-out test after exposure to high temperatures were between 0.65 and 0.68, 0.65

Preprints (www.preprints.org) | NOT PEER-REVIEWED | Posted: 17 January 2024 doi:10.20944/preprints202401.1291.v1

and 0.72, and 0.68 and 0.74, respectively. Compared with the specimens in Group A, the relative bond strength ratios of the specimens in Group C after 28 days of self-healing increased by 4.6%. Overall, the relative bond strength ratio of the secondary pull-out test results of Group C was higher than that of Group A and Group B. This result once again means that the healing method with an ambient temperature of 40 °C and a two-day cycle had a better effect.

Table 5. Results of the secondary pull-out test of the unhealed LWAC after exposure to high temperatures.

Group	BS at RT (MPa)	Residual BS (MPa)		Relative BS Ratio	
		300 °C	500 °C	300 °C	500 °C
Group A	27.99 (1.56)	18.89 (0.89)	18.17 (1.20)	0.68	0.65
Group B	28.38 (1.34)	20.48 (1.57)	18.35 (1.24)	0.72	0.65
Group C	28.02 (0.40)	20.70 (1.46)	19.00 (0.58)	0.74	0.68

Note: BS: bond strength; RT: room temperature.

In summary, for specimens that did not heal themselves after being exposed to high temperatures, there were some differences in the residual bond strength between the first and secondary pull-out tests between the control group and the experimental group. This is attributed to the fact that the high-temperature test did not cause serious degradation of the internal composition of the concrete in each group of specimens. However, the damage caused during the first pull-out test was more severe. The experimental group healed itself in a better environment, resulting in a significant improvement in the residual bond strength in the secondary pull-out test.

3.2.3. Local Bond–Slip Relationship and Bond Strength in Healed LWAC after Exposure to High Temperatures

The results of the pull-out test were all rebar pull-out failures after exposure to a temperature of 300 °C and being subjected to healing, as shown in Figure 12. The corresponding τ–s relationship curve is shown in Figure 13. The τ–s relationship curve of the first pull-out test of the healed specimen after 300 °C could be divided into linear ascending, non-linear ascending, and descending stages. As shown in Figure 13a, after 28 days of healing, the peak bond stresses of the experimental group and the control group were similar, and the corresponding slip to the peak bond stress was very small, about 0.5–1 mm. In contrast, as shown in Figure 13b, after 90 days of healing, the peak bond stress of Group C was higher than that of Group A, and the corresponding slip to the peak bond stress was approximately 1–1.5 mm. From this point of view, the improvement of the peak bond stress in Group C was better after 90 days of healing. Moreover, after the 28-day healing of the first pull-out specimen, the τ–s relationship curve of the secondary pull-out test still went through the four stages described previously. On the other hand, after 28 days of healing, the peak bond stress of Group C in the secondary pull-out test was slightly higher than that of Group A. However, after 90 days of healing, the peak bond stress of Group C in the secondary pull-out test was significantly higher than that of Group A.

Group A Group B Group C

(a)

Preprints (www.preprints.org) | NOT PEER-REVIEWED | Posted: 17 January 2024 doi:10.20944/preprints202401.1291.v1

Figure 12. Pull-out failure of healed LWAC specimens after exposure to a temperature of 300 °C: (a) a healing age of 28 days; (b) a healing age of 90 days.

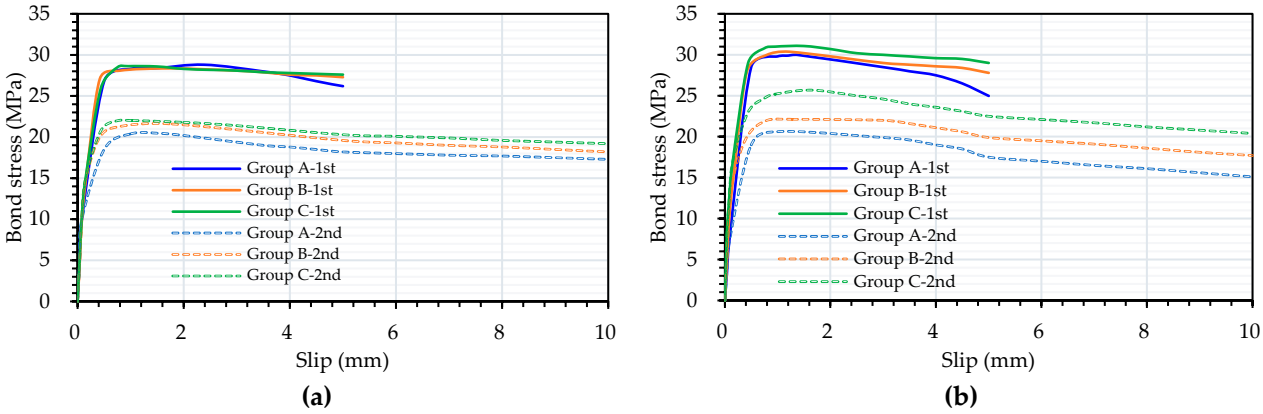

Figure 13. Local bond stress–slip relationship curves of healed LWAC specimens after exposure to 300 °C: (a) a healing age of 28 days; (b) a healing age of 90 days.

After being subjected to a temperature of 300 °C, the τ–s relationship curves of the Group A specimens under different healing age conditions are shown in Figure 14. As shown in Figure 14, with the increase in healing age, the peak bond stress of the Group A specimens increased significantly. In addition, with the increase in the healing age, the peak bond stress of the secondary pull-out test in Group A also increased.

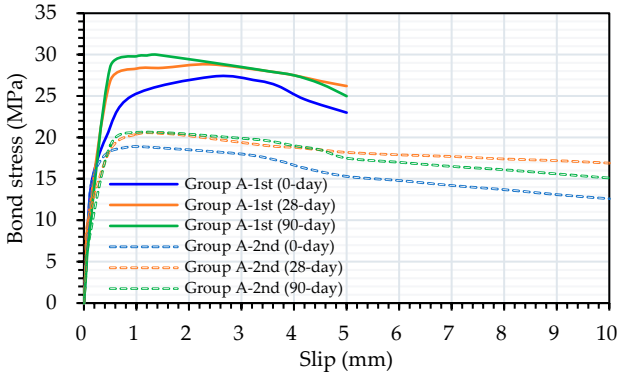

Figure 14. Local bond stress–slip relationship curves of healed Group A specimens after different healing ages.

Moreover, the τ–s relationship curves of the experimental group specimens at different healing ages after being subjected to a temperature of 300 °C are shown in Figure 15. As shown in Figure 15a, with the increase in the healing age, the peak bond stress of the Group B specimens increased significantly. In addition, with the increase in the healing age, the peak bond stress of the secondary pull-out test in Group B also increased. As shown in Figure 15b, with the increase in the healing age, the peak bond stress of Group C specimens increased significantly. In addition, with the increase in the healing age, the peak bond stress of the secondary pull-out test in Group C also increased

Preprints (www.preprints.org) | NOT PEER-REVIEWED | Posted: 17 January 2024 doi:10.20944/preprints202401.1291.v1

significantly. As shown in Figures 9 and 13, the slip of the experimental group was slightly smaller than that of the control group when the maximum load occurred, and this phenomenon showed the same trend in each healing age and target temperature. In addition, as shown in Figures 14 and 15, the trends of Group A at the healing ages of 28 days and 90 days were similar. This result shows that the hydration reaction of the cement itself had been roughly developed in 28 days, and there was no obvious increase in late age. In contrast, it was found that, with age, the bond strength of Group C showed a more obvious improvement. This was especially true in the secondary pull-out test, where the repair rate was higher when the healing age was 90 days. From this perspective, the curing method of Group C was more effective.

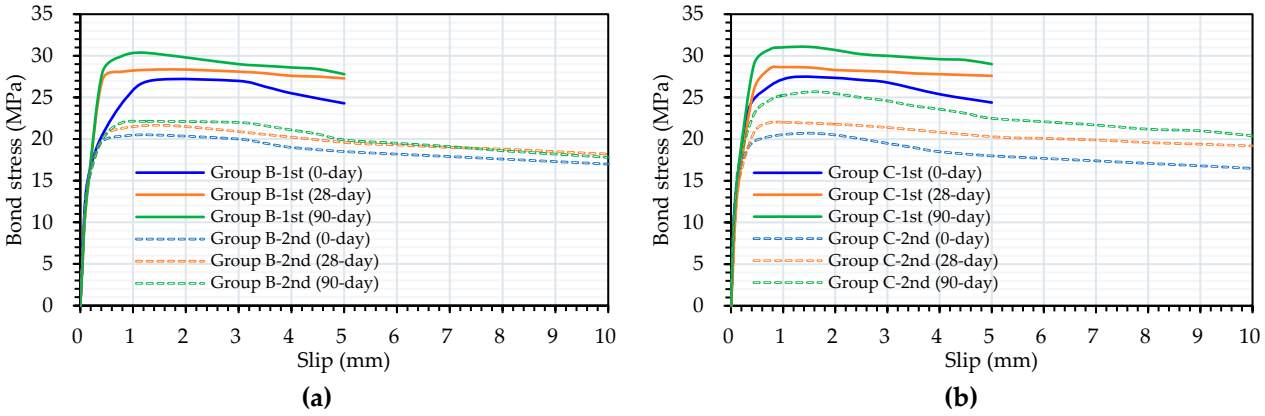

Figure 15. Local bond stress–slip relationship curves of the healed experimental group after different healing ages: (a) Group B; (b) Group C.

The pull-out test results of the healed specimens after exposure to a temperature of 300 °C are shown in Table 6. As shown in Table 6, after 28 days of self-healing, the bond strengths of Group A, Group B, and Group C were 28.82, 28.36, and 28.64 MPa, respectively. After 90 days of self-healing, the bond strengths of Group A, Group B, and Group C were 29.99, 30.37, and 31.08 MPa, respectively. In addition, for the specimens of different self-healing ages after 300 °C, the relative bond strength ratio was calculated based on the bond strength without self-healing after 300 °C, and the results are shown in Table 6. As shown in Table 6, the relative bond strength ratios of Group A, Group B, and Group C after 28 days and 90 days of self-healing were 1.05 and 1.10, 1.05 and 1.12, and 1.05 and 1.13, respectively. Compared with the specimens in Group A, the relative bond strength ratios of the specimens in Group B and Group C after 28 days of self-healing decreased by 0.6% and 0.8%, respectively. Compared with the specimens in Group A, the relative bond strength ratios of the specimens in Group B and Group C after 90 days of self-healing increased by 2.3% and 3.4%, respectively. In terms of self-healing for 90 days, the relative bond strength ratio of Group C was the highest, which again proved that the curing method with a curing temperature of 40 °C and a two-day cycle was better.

Table 6. Residual bond strength and relative bond strength ratios of the healed LWAC after exposure to a temperature of 300 °C.

Group	Unhealed BS (MPa)	Residual BS (MPa)		Relative BS Ratio	
		28 days of self-healing	90 days of self-healing	28 days of self-healing	90 days of self-healing
Group A	27.35 (0.68)	28.82 (0.55)	29.99 (1.19)	1.05	1.10
Group B	27.07 (1.14)	28.36 (2.23)	30.37 (0.63)	1.05	1.12
Group C	27.41 (0.69)	28.64 (0.32)	31.08 (0.72)	1.05	1.13

Note: BS: bond strength.

Moreover, each group of specimens exposed to a temperature of 300 °C that underwent different self-healing ages and were damaged in the first pull-out test were allowed to self-heal for another 28

Preprints (www.preprints.org) | NOT PEER-REVIEWED | Posted: 17 January 2024 doi:10.20944/preprints202401.1291.v1

days. As shown in Figure 16, the results of the secondary pull-out test after self-healing for 28 days were analyzed.

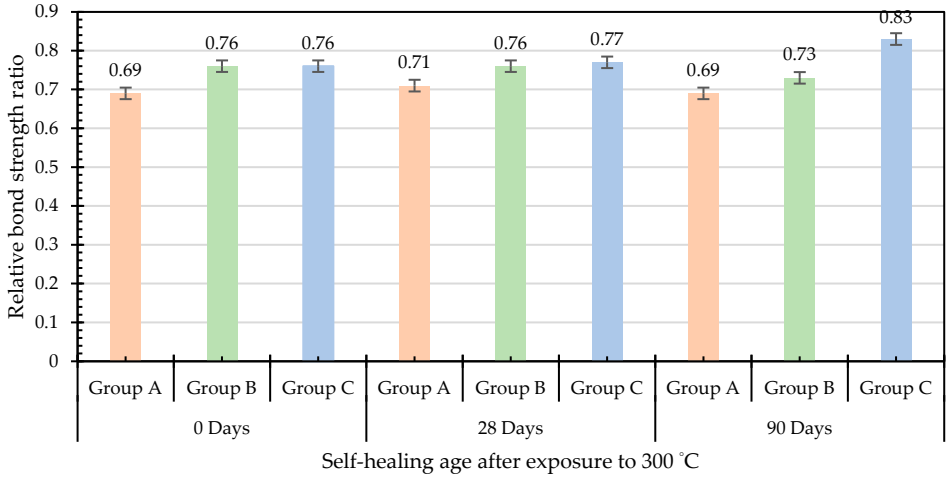

Figure 16. Secondary relative bond strength ratio of the healed specimens after they were exposed to a temperature of 300 °C and damaged in the first pull-out test.

As shown in Figure 16, after 300 °C, at the healing ages of 0, 28, and 90 days, the relative bond strength ratios of the secondary pull-out test results of Group A, Group B, and Group C were 0.69, 0.76, and 0.76; 0.71, 0.76, and 0.77; and 0.69, 0.73, and 0.83, respectively. Compared with the specimens in Group A, the relative bond strength ratios of the specimens in Group B and Group C after 90 days of self-healing increased by 5.8% and 20.3%, respectively. In comparison, the relative bond strength ratio of the secondary pull-out test results of Group B and Group C was higher than that of Group A.

In summary, for the specimens that healed themselves after being exposed to high temperatures, there was a significant difference in the residual bond strength between the first and secondary pull-out tests of Group A and Group C. This is attributed to the fact that the high-temperature test did not cause serious degradation of the internal composition of the concrete in the two groups of specimens. However, the damage caused by the first pull-out test was relatively severe. Group C healed itself in a better environment, making its residual bond strength in the secondary pull-out test significantly better than that of Group A.

3.3. The Results of the Concrete Crack-Healing Observation

The crack-healing conditions on the surface of the pull-out specimens were observed. Due to the specimens being damaged by rebar pull-out, only minor cracks were produced on their surfaces. To understand the self-healing of concrete cracks with age in the pull-out specimens exposed to high temperatures, a specific crack was selected on the surface of the specimen and observed using a crack-width-measuring instrument. For each group of LWAC specimens that developed cracks after exposure to high temperatures, an initial crack was selected and a photo was taken. After that, the specimens in each group healed themselves according to the planned healing method. At each planned self-healing age, the healing status of the selected cracks was observed and photographed. Figure 17 shows the microscopic images of the surface cracks of the pull-out specimens of each group of LWACs at different self-healing ages after exposure to temperatures of 300 °C and 500 °C. As shown in Figure 17, after exposure to a temperature of 300 °C, Group C began to exhibit obvious calcium carbonate crystal deposition on both sides of the crack at the age of seven days. In addition, the distribution of calcium carbonate crystal particles was visible on the surface around the crack. In contrast, only sporadic calcium carbonate particles appeared in the cracks in Group A and Group B. The crystallization of Group C reached its peak on the 14th day of the self-healing age, as was visible to the naked eye. The interior of the cracks was more or less filled with calcium carbonate crystals and tended to gradually expand outward. However, for Group A and Group B, there was no significant difference from the situation at the self-healing age of seven days. Then, at the self-healing

Preprints (www.preprints.org) | NOT PEER-REVIEWED | Posted: 17 January 2024 doi:10.20944/preprints202401.1291.v1

age of 21 days, it was found that the concrete surface of Group C exhibited some peeling off of the surface. This may be due to the long-term soaking in the curing solution causing some slight erosion damage to the concrete surface. However, when the healing time was extended to 28 days, calcium carbonate crystal crystallization again occurred on the surface of Group C. It is speculated that, as the age increased, the calcium carbonate crystals continued to penetrate deep into the interior of the specimen to crystallize, causing tension damage near the surface and falling off. This inference is consistent with the results of the compression test and pull-out test of Group C, which show better strength performance with increasing age. Furthermore, more granular crystal accumulation can be seen in the cracks of Group A and Group B. Although the deposition rate was slower, there was still a continuous reaction. After exposure to a temperature of 500 °C, with the increase in the self-healing age, the crystallization of calcium carbonate in Group A and Group B was not obvious, with only fairly sparse granular crystals. In comparison, Group C showed crystallization at the self-healing age of seven days. However, compared with the situation at 300 °C, the crystals were fine and localized. At the age of 14 days, the healing of Group C underwent relative growth and began to develop outwards and widely. There was a better repair trend at the self-healing ages of 21 and 28 days, but there was still some surface peeling on the concrete surface.

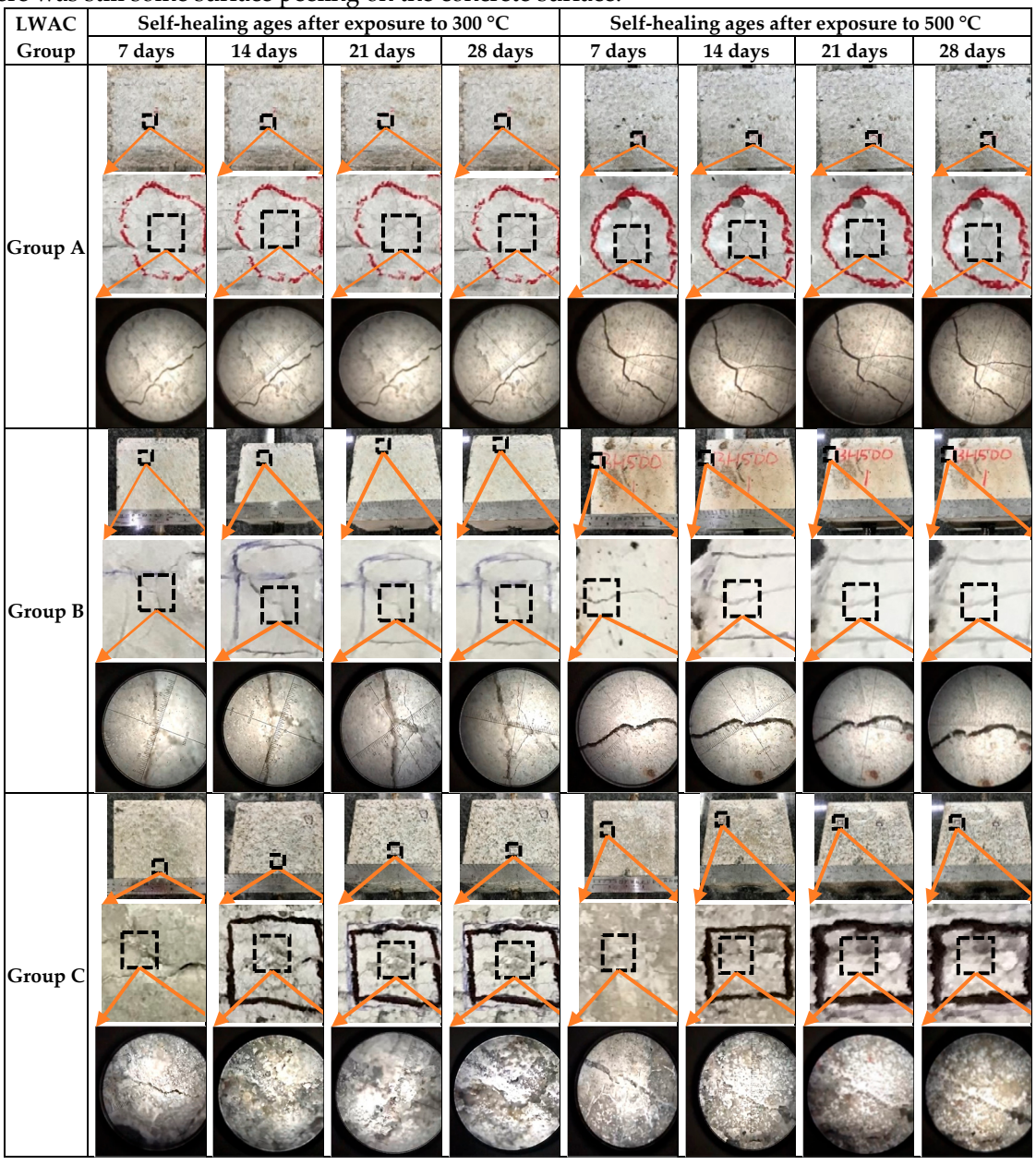

Figure 17. Microscopic images of the crack healing of the pull-out specimens at different self-healing ages.

Preprints (www.preprints.org) | NOT PEER-REVIEWED | Posted: 17 January 2024 doi:10.20944/preprints202401.1291.v1

3.4. The Results of FESEM, EDS, and XRD Analysis

When exposed to high temperatures, concrete undergoes a series of changes in its chemical composition and physical structure. Due to changes in the morphology of these hydration products, concrete gradually and sometimes dramatically loses its mechanical strength and durability [48]. Essentially, when exposed to high temperatures, concrete can change its microstructure through appropriate curing, thereby affecting its mechanical properties [49].

3.4.1. Results of the FESEM images

The FESEM images of the LWAC samples are shown in Figure 18. The figure shows that there were many fine pores inside the LWAs. Porosity and pore size distribution are the main factors controlling the strength of concrete [46]. At room temperature, the calcium carbonate crystal particles in the Group C sample had a parallel polygonal cubic structure mixed with some spherical structures, as shown in Figure 18a. Therefore, it is speculated that there were a large number of calcium carbonate deposits. In other words, Group C specimens exhibited microbially induced calcium carbonate precipitation, thereby achieving better repair and healing effects and improving their performance. This is consistent with the results of Kadapure and Deshannavar [50]. Phillips et al. [51] pointed out that during the MICP process, the metabolic activity of microorganisms increased the local saturation state of bacterial cells, thereby promoting the precipitation of $CaCO_3$. After the high-temperature treatment, Group C had a relatively dense structure around the ITZ at 300 °C, as shown in Figure 18b. While the ITZ at 500 °C was relatively loose, multiple small cracks could be seen around the matrix. Furthermore, the high-temperature environment of 500 °C indeed caused the hydrated C-S-H colloid to lose its bound water and undergo chemical changes. Due to the high temperatures, parts of the ettringite and C-S-H colloid were destroyed and dispersed, resulting in the texture of the block having a smoother appearance, as shown in Figure 18c.

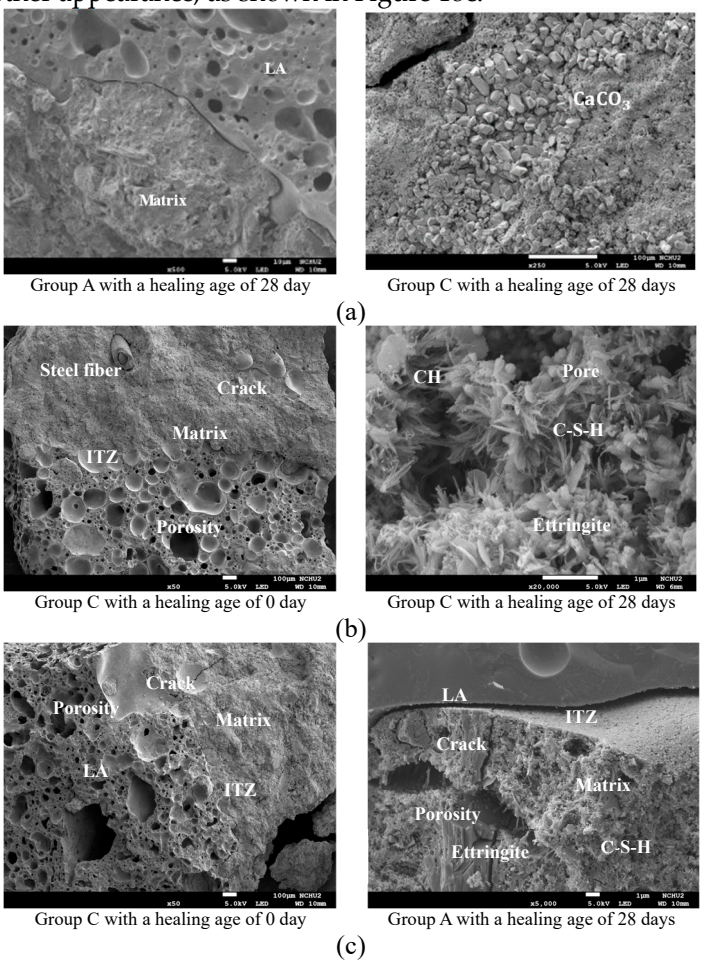

Figure 18. FESEM images of the surface blocks of LWAC samples: (a) at room temperature; (b) after exposure to a temperature of 300 °C; and (c) after exposure to a temperature of 500 °C.

Preprints (www.preprints.org) | NOT PEER-REVIEWED | Posted: 17 January 2024 doi:10.20944/preprints202401.1291.v1

3.4.2. Results of the EDS analysis

For each group of LWAC samples exposed to room temperature and high temperatures, after 28 days of self-healing, EDS was used to analyze the weight percentage of various chemical elements on their surface and central blocks. The EDS spectra of each group of samples at different ambient temperatures are shown in Figures 19–21. The EDS analysis indicated that as the ambient temperature and sampling location varied, the main elements (weight percentage) in the sample also varied. Overall, the elements contained in each group of samples were mainly C, O, and Ca. In addition, some samples also contained Mg, Al, Si, K, Fe, S, and Na elements. Observing the samples of Group C, it can be seen that after 28 days of self-healing, Ca, C, and O bonded to form $CaCO_3$ and filled the crack area. It can be concluded that the large number of polygonal blocks observed in the previous FESEM images were calcium carbonate crystals. This result also confirmed that microbial mineralization occurred in the samples of Group C. In addition, this is consistent with the results of Kadapure and Deshannavar [50]. Therefore, Group C achieved a better performance than Group A. In the case of a high temperature of 500 °C, compared with the block in the center, there is a large difference in the amount of calcium carbonate deposition in the blocks at the edges. This corroborated the inference that the strains near the surface of the test specimen died at a high temperature of 500 °C and that the strains inside could partially survive. Furthermore, this is consistent with the results of the compression test and the pull-out test. The EDS analysis results showed that there were bacterial $CaCO_3$ crystals in the samples of the experimental group. In other words, EDS verified the formation of calcium carbonate in the experimental group samples. It is worth noting that a higher percentage of calcium was found in the experimental group samples. The atomic ratio of calcium to silicon can be used to reflect the changes in the chemical composition of C-S-H colloids in ITZ and the cement matrix and is also an important indicator in distinguishing the rich phase of hydration products [52]. As shown in Figure 21, in the Group A sample, the Ca/Si ratio was 0.04; in the Group B sample, the Ca/Si ratio was 0.07; and, in the Group C sample, the Ca/Si ratio was 0.26.

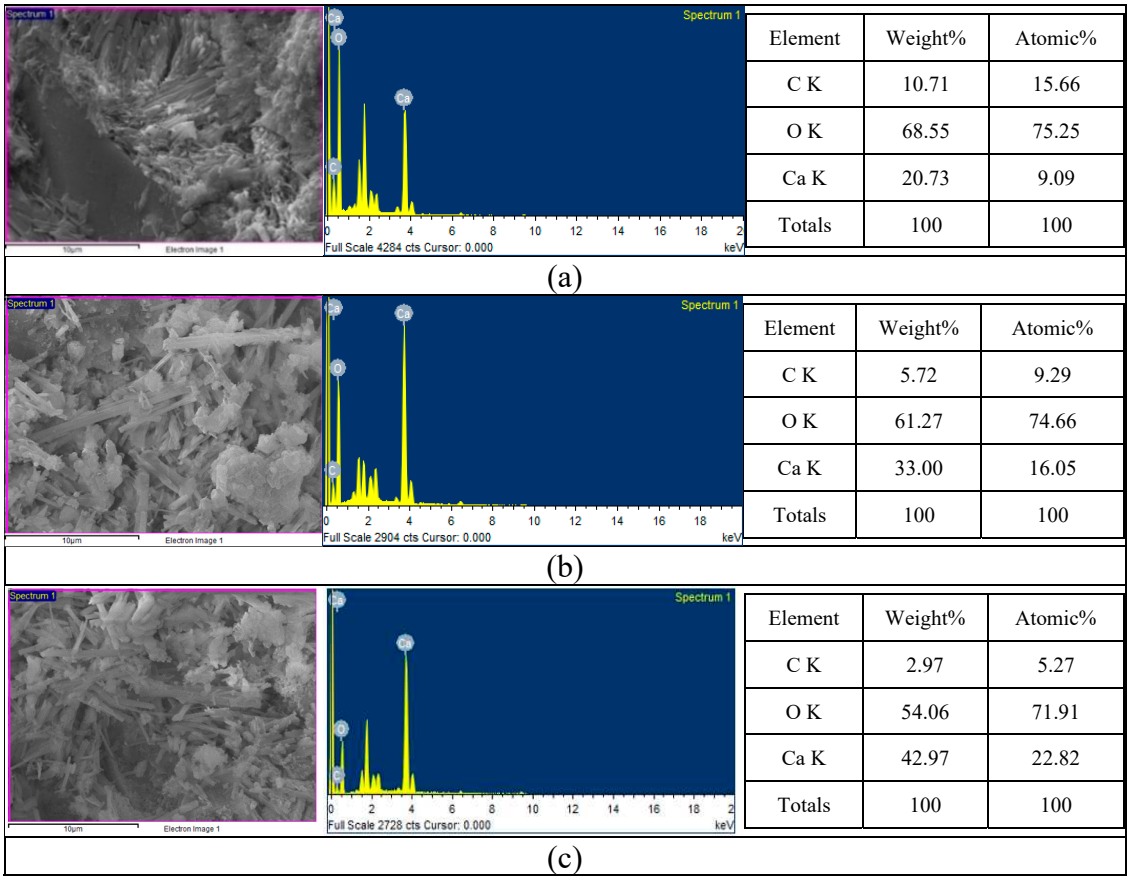

Element	Weight%	Atomic%
C K	10.71	15.66
O K	68.55	75.25
Ca K	20.73	9.09
Totals	100	100

Element	Weight%	Atomic%
C K	5.72	9.29
O K	61.27	74.66
Ca K	33.00	16.05
Totals	100	100

Element	Weight%	Atomic%
C K	2.97	5.27
O K	54.06	71.91
Ca K	42.97	22.82
Totals	100	100

Figure 19. EDS analysis of the center block of each group of samples (after being subjected to 300 °C and with a healing period of 28 days): (a) Group A; (b) Group B; and (c) Group C.

Preprints (www.preprints.org) | NOT PEER-REVIEWED | Posted: 17 January 2024 doi:10.20944/preprints202401.1291.v1

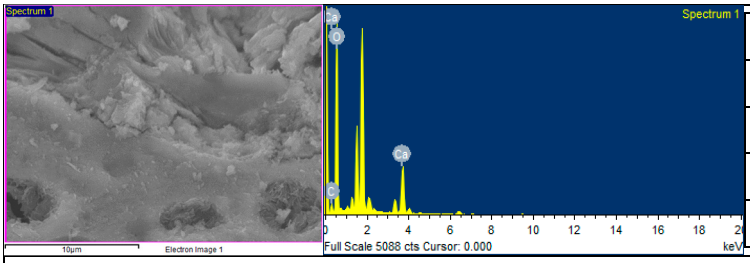

Element	Weight%	Atomic%
C K	4.33	6.20
O K	81.78	87.84
Ca K	13.89	5.96
Totals	100	100

(a)

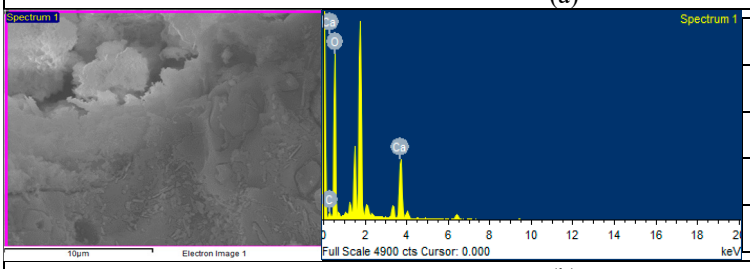

Element	Weight%	Atomic%
C K	2.94	4.34
O K	79.19	87.76
Ca K	17.87	7.91
Totals	100	100

(b)

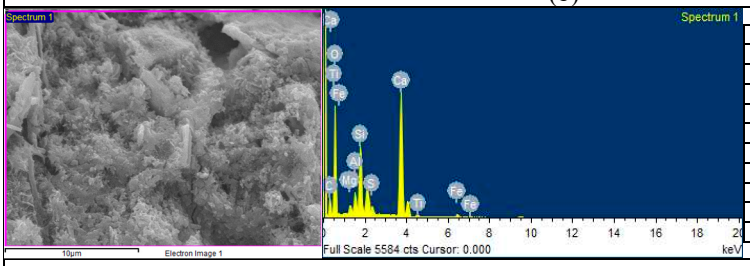

Element	Weight%	Atomic%
C K	8.33	13.52
O K	54.71	66.63
Mg K	0.79	0.64
Al K	1.83	1.32
Si K	6.68	4.63
S K	1.11	0.67
Ca K	24.10	11.72
Ti K	0.34	0.14
Fe K	2.12	0.74
Totals	100	100

(c)

Figure 20. EDS analysis of the center block of each group of samples (after being subjected to a temperature of 500 °C and with a healing period of 28 days): (a) Group A; (b) Group B; and (c) Group C.

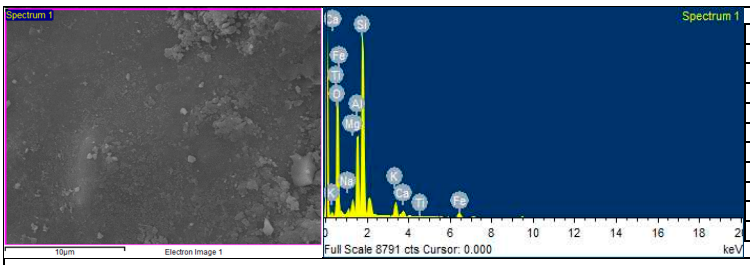

Element	Weight%	Atomic%
O K	51.79	66.75
Na K	0.82	0.74
Mg K	1.90	1.61
Al K	9.66	7.38
Si K	26.10	19.16
K K	3.39	1.79
Ca K	1.45	0.75
Ti K	0.38	0.16
Fe K	4.51	1.66
Totals	100	100

(a)

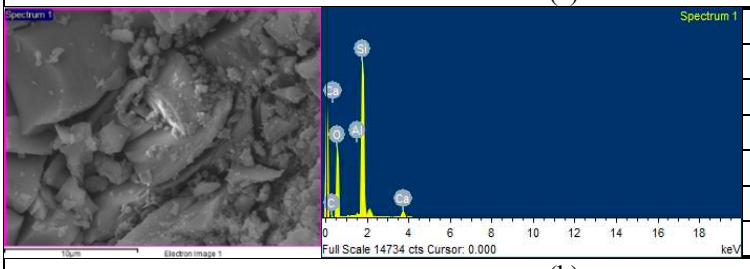

Element	Weight%	Atomic%
C K	6.27	9.89
O K	54.25	64.20
Al K	0.34	0.24
Si K	35.62	24.01
Ca K	3.51	1.66
Totals	100	100

(b)

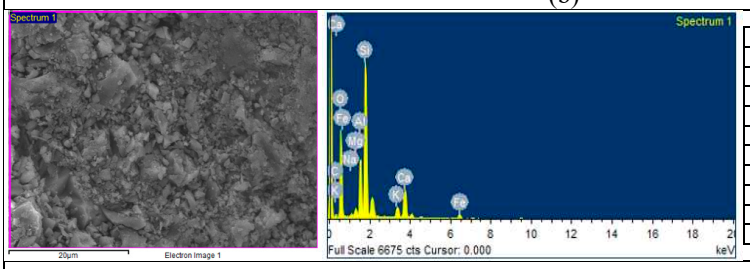

Element	Weight%	Atomic%
C K	5.84	9.89
O K	46.81	59.48
Na K	0.44	0.39
Mg K	1.05	0.88
Al K	7.29	5.49
Si K	22.72	16.44
K K	2.83	1.47
Ca K	8.57	4.34
Fe K	4.45	1.62
Totals	100	100

(c)

Figure 21. EDS analysis of the near-surface blocks of each group of samples (after being subjected to a temperature of 500 °C and with a healing period of 28 days): (a) Group A; (b) Group B; and (c) Group C.

Preprints (www.preprints.org) | NOT PEER-REVIEWED | Posted: 17 January 2024 doi:10.20944/preprints202401.1291.v1

3.4.3. Results of the XRD Analysis

As shown in Figure 22, the XRD analysis indicated that the main reflection angles (2-theta) of the calcium carbonate crystal were 30.6°, 36.5°, and 43.1°. This has also been observed in previous studies [33]. Regardless of the target temperature, the X-ray reflected energy intensity of Groups B and C at all angles was higher than that of Group A. As for the quartz crystal, its main reflection angles were 20.8° and 26.5°. In addition, the main reflection angles of CH crystals were found to be 18.0° and 34.1°. At different temperatures, the X-ray reflection energy intensity of Groups B and C at all angles was lower than that of Group A. In essence, the composition of the CH crystal structure is relatively loose, and its contribution to the strength of concrete is less significant. It can be seen from the test results of the experimental group that adding the *S. pasteurii* strain could effectively reduce the formation of CH crystals and convert them into cubic crystals and agglomerated substances. This can well illustrate that the experimental group indeed showed higher strength in the pull-out test.

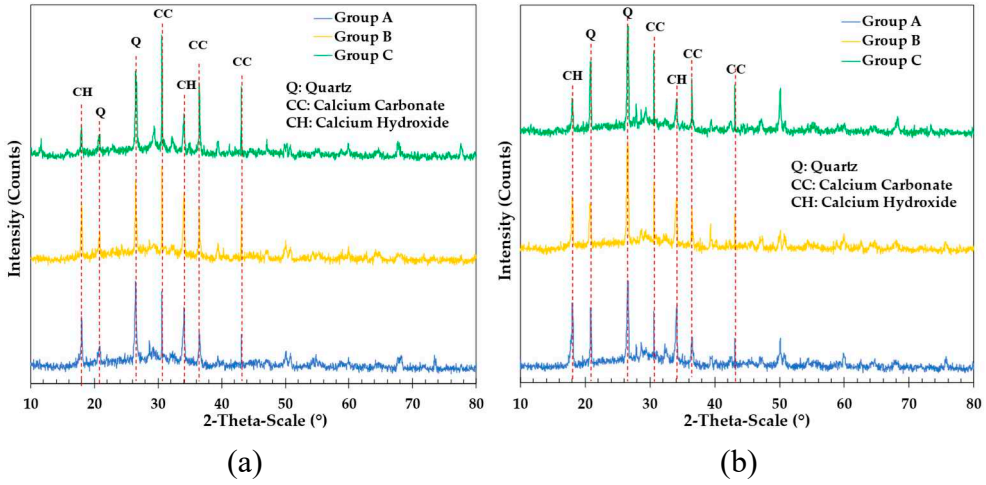

Figure 22. XRD analysis of the center block of each group of samples with a healing period of 28 days: (a) after exposure to 300 °C; (b) after exposure to 500 °C.

4. Conclusions

In this study, biomineralization technology was applied to improve the bond strength of fiber-reinforced LWAC after exposure to high temperatures. The test results verified that biomineralization can effectively improve the bond strength of LWAC after exposure to temperatures of 300 °C and 500 °C. After being exposed to a temperature of 300°C and undergoing self-healing for 90 days, compared with the specimens in Group A, the relative bond strength ratios of the secondary pull-out tests of the specimens in Groups B and C increased by 5.8% and 20.3%, respectively. After high-temperature action, the τ–s relationship curve of each group of concrete pull-out specimens during the first pull-out could be divided into linear ascending, non-linear ascending, and descending stages. As the healing age increased, the bond strength of Group C increased significantly. In the secondary pull-out test, the 90-day healing period had a higher repair rate, which confirmed that the biomineralization curing method of Group C was more effective. Group A and Group B were healed in a constant-temperature incubator, and there was no significant difference in the bond strength after self-healing. This is because the high temperatures caused the bacterial strain of Group B to be lost, resulting in less obvious mineralization. Additionally, strains mineralize slowly in the absence of adequate nutrient sources. In contrast, biomineralization in Group C operated effectively due to the provision of nutrient sources. Its EDS and XRD analysis results confirmed that the precipitate formed at the crack was calcium carbonate, which improved the bond strength after self-healing. As a result, the test results of Group C were better than those of Group A and Group B.

Author Contributions: Conceptualization, H.-J.C. and C.-W.T.; methodology, H.-J.C. and C.-W.T.; software, C.-W.T. and H.-W.C.; validation, H.-J.C. and Y.-H.L.; formal analysis, C.-W.T.; investigation, H.-J.C. and Y.-H.L.; resources, C.-W.T.; data curation, H.-J.C., H.-W.C., and Y.-H.L.; writing—original draft preparation, H.-J.C. and

C.-W.T.; writing—review and editing, C.-W.T.; visualization, H.-W.C.; supervision, C.-W.T. and Y.-H.L.; project administration, C.-W.T.; funding acquisition, C.-W.T. All authors have read and agreed to the published version of the manuscript.

Funding: This research was funded by the Ministry of Science and Technology of Taiwan, grant number MOST 110-2221-E-230-001-MY3.

Institutional Review Board Statement: Not applicable.

Informed Consent Statement: Not applicable.

Data Availability Statement: The data presented in this study are available upon request from the corresponding author.

Acknowledgments: The authors are grateful to the Department of Civil Engineering of National Chung-Hsing University for providing the experimental equipment and technical support. In addition, the authors thank Yi-Hao Guo from the Chunmin Construction Company for providing bacterial solutions and technical support.

Conflicts of Interest: The authors declare no conflicts of interest.

References

1. Tang, C.-W. Uniaxial bond stress-slip behavior of reinforcing bars embedded in lightweight aggregate concrete. Structural Engineering and Mechanics 2017, 62(5), 651–661. https://doi.org/10.12989/sem.2017.62.5.651
2. Gao, J.; Suqa, W.; Morino, K. Mechanical properties of steel fiber-reinforced, high-strength, lightweight concrete. Cem Concr Compos. 1997, 19, 307–313. https://doi.org/10.1016/S0958-9465(97)00023-1
3. Guneyisi, E.; Gesoglu, M.; Azez, O.A.; Öz, H.Ö. Effect of nano silica on the workability of self-compacting concretes having untreated and surface treated lightweight aggregates. *Construct. Build. Mater.* **2016**, *115*, 371–380. https://doi.org/10.1016/j.conbuildmat.2016.04.055
4. Inozemtcev, A.S.; Epikhin, S.D. Conditions for the Preparation of Self-Compacting Lightweight Concrete with Hollow Microspheres. *Materials* **2023**, *16*, 7288. https://doi.org/10.3390/ma16237288
5. Bicer, A.; Celik, N.; Ozgen, F.; Kistak, C.; Taskiran, A. Thermomechanical Properties of a Concrete Composed of Cherry Tree Resin and Expanded Clay (Exclay) Aggregate. *Appl. Sci.* **2024**, *14*, 336. https://doi.org/10.3390/app14010336
6. Stratoura, M.C.; Lazari, G.-E.D.; Badogiannis, E.G.; Papadakis, V.G. Perlite and Rice Husk Ash Re-Use As Fine Aggregates in Lightweight Aggregate Structural Concrete—Durability Assessment. *Sustainability* **2023**, *15*, 4217. https://doi.org/10.3390/su15054217
7. Youssf, O.; Roychand, R.; Elchalakani, M.; Tahwia, A.M. Assessment of the Efficiency of Eco-Friendly Lightweight Concrete as Simulated Repair Material in Concrete Joints. *Buildings* **2024**, *14*, 37. https://doi.org/10.3390/buildings14010037
8. Różycki, M.; Hager, I.; Zdeb, T.; Sitarz, M.; Mróz, K.; Zdeb, J.; Smorońska, N. Mechanical Properties and Water Permeability of Textile-Reinforced Reactive Powder Concrete with Lightweight Aggregate. *Materials* **2023**, *16*, 7619. https://doi.org/10.3390/ma16247619
9. Chen, H.-J.; Chen, T.-K.; Tang, C.-W.; Chang, H.-W. The Evaluation of the Effectiveness of Biomineralization Technology in Improving the Strength of Damaged Fiber-Reinforced LWAC. *Materials* **2024**, *17*, 214. https://doi.org/10.3390/ma17010214
10. Zhao, M.; Zhao, M.; Chen, M.; Li, J.; Law, D. An experimental study on strength and toughness of steel fiber reinforced expanded-shale lightweight concrete. *Constr. Build. Mater.* **2018**, *183*, 493–501. https://doi.org/10.1016/j.conbuildmat.2018.06.178
11. Kovács, T.; Gyurkó, Z.; Jakab, L.; Nemes, R. Influence of Unidirectional Cyclic Loading on Bond between Steel Bars Embedded in Lightweight Aggregate Concrete. *Solids* **2022**, *3*, 397-415. https://doi.org/10.3390/solids3030028
12. Abed, M.A.; Alkurdi, Z.; Fořt, J.; Černý, R.; Solyom, S. Bond Behavior of FRP Bars in Lightweight SCC under Direct Pull-Out Conditions: Experimental and Numerical Investigation. *Materials* **2022**, *15*, 3555. https://doi.org/10.3390/ma15103555
13. Solyom, S.; Di Benedetti, M.; Balázs, G.L. Bond of FRP bars in air-entrained concrete: Experimental and statistical study. *Constr.Build. Mater.* **2021**, *300*, 124193. https://doi.org/10.1016/j.conbuildmat.2021.124193
14. Solyom, S.; Balázs, G.L. Analytical and statistical study of the bond of FRP bars with different surface characteristics. *Compos. Struct.* **2021**, *270*, 113953. https://doi.org/10.1016/j.compstruct.2021.113953
15. Huang, L.; Chi, Y.; Xu, L.; Chen, P.; Zhang, A. Local bond performance of rebar embedded in steel-polypropylene hybrid fiber reinforced concrete under monotonic and cyclic loading. *Constr. Build. Mater.* **2016**, *103*, 77–92. https://doi.org/10.1016/j.conbuildmat.2015.11.040
16. ACI Committee 408. Bond and development of straight reinforcing bars in tension (ACI 408R–03). Farmington Hills, MI: American Concrete Institute; 2003.

17. ACI Committee 318-19. Building Code Requirements for Structural Concrete and Commentary. American Concrete Institute, Farmington Hills (2019).
18. Hossain, K.M.A. Bond characteristics of plain and deformed bars in lightweight pumice concrete. *Constr. Build. Mater.* **2008**, *22(7)*, 1491–2149. https://doi.org/10.1016/j.conbuildmat.2007.03.025
19. Mo, K.H.; Alengaram, U.J.; Visintin, P.; Goh, S.H.; Jumaat, M.Z. Influence of lightweight aggregate on the bond properties of concrete with various strength grades. *Constr. Build. Mater.* **2015**, *84*, 377–386. https://doi.org/10.1016/j.conbuildmat.2015.03.040
20. CEB-FIP. Fib Model Code for Concrete Structures 2010; Comité Euro international du Béton/Federation Internationale de la Precontrainte: Lausanne, Switzerland, 2013.
21. Wang, B.; Zhu, E.; Zhang, Z.; Zhu, C. Bond-slip behaviour of lightweight aggregate concrete based on virtual crack model with exponential softening characteristics. *Constr. Build. Mater.* **2022**, *345*, 128349. https://doi.org/10.1016/j.conbuildmat.2022.128349
22. Liu, Y.; Liu, X.; Wu, T.; Luo, X.; Feng, W. Bond-slip behavior between corroded rebar and lightweight aggregate concrete. *Constr. Build. Mater.* **2023**, *367*, 130268. https://doi.org/10.1016/j.conbuildmat.2022.130268
23. Yang, X.; Wu, T.; Liu, X.; Liu, Y. Bond-slip relationship of rebar in lightweight aggregate concrete. *Structures* **2022**, *45*, 2198–2209. https://doi.org/10.1016/j.istruc.2022.10.010
24. Varghese, A.; Anand, N.; Arulraj, G.P.; Alengaram, U.J. Influence of fibers on bond strength of concrete exposed to elevated temperature. *J. Adhe. Sci. Tech.* **2019**, *33*, 1521–1543, https://doi.org/10.1080/01694243.2019.1602889.
25. Kevinly, C.; Du, P.; Tan, K.H. Local bond-slip behaviour of reinforcing bars in fibre reinforced lightweight aggregate concrete at ambient and elevated temperatures. *Constr. Build. Mater.* **2023**, *377*, 131010. https://doi.org/10.1016/j.conbuildmat.2023.131010
26. Tang, C.-W. Local bond–slip behavior of fiber reinforced LWAC after exposure to elevated temperatures. *Structural Engineering and Mechanics* **2020**, *73(4)*, 437–445. https://doi.org/10.12989/sem.2020.73.4.437
27. Hermawan, H.; Wiktor, V.; Gruyaert, E.; Serna, P. Experimental investigation on the bond behaviour of steel reinforcement in self-healing concrete. *Constr. Build. Mater.* **2023**, *383*, 131378. https://doi.org/10.1016/j.conbuildmat.2023.131378
28. Dry, C.M. Three designs for the internal release of sealants, adhesives, and waterproofing chemicals into concrete to reduce permeability. *Cem. Concr. Res.* **2000**, *30*, 1969–1977. https://doi.org/10.1016/S0008-8846(00)00415-4
29. Stanaszek-Tomal, E. Bacterial Concrete as a Sustainable Building Material?. *Sustainability* **2020**, *12*, 696. https://doi:10.3390/su12020696
30. Jonkers, H.M.; Thijssen, A.; Muyzer, G.; Copuroglu, O.; Schlangen, E. Application of bacteria as self-healing agent for the development of sustainable concrete. *Ecol. Eng.* **2010**, *36*, 230–235. https://doi.org/10.1016/j.ecoleng.2008.12.036
31. Xu, J.; Wang, X.; Zuo, J.; Liu, X. Self-healing of concrete cracks by ceramsite-loaded microorganisms. *Adv. Mater. Sci. Eng.* **2018**, 2018, 5153041. https://doi.org/10.1155/2018/5153041.
32. Nimafar, M.; Samali, B.; Hosseini, S.J.; Akhlaghi, A. Use of Bacteria Externally for Repairing Cracks and Improving Properties of Concrete Exposed to High Temperatures. *Crystals* **2021**, *11*, 1503. https://doi.org/10.3390/cryst11121503
33. Chen, H.-J.; Chang, H.-L.; Tang, C.-W.; Yang, T.-Y. Application of biomineralization technology to self-healing of fiber-reinforced lightweight concrete after high temperatures. *Materials* **2022**, *15(21)*, 7796. https://doi.org/10.3390/ma15217796
34. Krishnapriya, S.; Babu, D.L.V.; Arulraj, G.P. Isolation and identification of bacteria to improve the strength of concrete. *Microbiol. Res.* **2015**, *174*, 48–55.
35. Wiktor, V.; Jonkers, H.M. Case Studies in Construction Materials Field performance of bacteria-based repair system: Pilot study in a parking garage. *Case Stud. Constr. Mater.* **2015**, *2*, 11–17.
36. De Muynck, W.; Verstraete, W. Bacterial carbonate precipitation as an alternative surface treatment for concrete. *Constr. Build. Mater.* **2008**, *22*, 875–885.
37. Chen, H.-J.; Peng, C.-F.; Tang, C.-W.; Chen, Y.-T. Self-Healing Concrete by Biological Substrate. *Materials* **2019**, *12*, 4099. https://doi.org/10.3390/ma12244099
38. Tang, C.-W. Local bond stress-slip behavior of reinforcing bars embedded in lightweight aggregate concrete. *Computers & Concrete* **2015**, *16(3)*, 449–466. https://doi.org/10.12989/cac.2015.16.3.449
39. Meng, L.; Zhang, C.; Wei, J.; Li, L.; Liu, J.; Wang, S.; Ding, Y. Mechanical properties and microstructure of ultra-high strength concrete with lightweight aggregate. *Case Stud. Constr. Mater.* **2023**, *18*, e01745. https://doi.org/10.1016/j.cscm.2022.e01745
40. Bremner, T.W.; Holm, T.A. Elastic compatibility and the behavior of concrete. *ACI J.* **1986**, *83*, 244–250. https://doi.org/10.14359/10422
41. Lu, J.X. Recent advances in high strength lightweight concrete: From development strategies to practical applications. *Constr. Build. Mater.* **2023**, *400*, 132905. https://doi.org/10.1016/j.conbuildmat.2023.132905.

42. Cairns, J.; Jones, K. An evaluation of the bond-splitting action of ribbed bars. *ACI Mater J* **1996**, *93(1)*, 10–9.
43. Harajli, M.H.; Hout, M.; Jalkh, W. Local bond stress-slip behaviour of reinforcing bars embedded in plain and fibre concrete. *ACI Mater. J.* **1995**, *92*, 343-353. https://doi.org/10.14359/999.
44. Shima, H.; Chou, L.L.; Okamura, H. Micro and macro models for bond in reinforced concrete. *J. Fac. Eng.* **1987**, *39*, 133–194.
45. Soroushian, P.; Mirza, F.; Alhozaimy, A. Bonding of confined steel fiber reinforced concrete to deformed bars. *ACI Mater. J.* **1994**, *91*, 144–149.
46. Metha, P.K.; Monteiro, P.J.M. *Concrete: Microstructure, Properties and Materials*, 3rd Ed.; McGraw-Hill: New York, NY, USA, 2006.
47. Siddique, R.; Kaur, D. Properties of concrete containing ground granulated blast furnace slag (GGBFS) at elevated temperatures. *J. Adv. Res*. **2012**, *3*, 45–51. https://doi.org/10.1016/j.jare.2011.03.004
48. Bazant, Z.P.; Kaplan, M.F. *Concrete at High Temperatures*. Longman Group, UK, 1996, pp. 1–20.
49. Wang, H.; Lyu, H.; Liu, T.; Li, Y.; Tan, K.H. Effect of post-fire curing on compressive strength of ultra-high performance concrete and mortar. *Constr. Build. Mater.* **2022**, *346*, 128447. https://doi.org/10.1016/j.conbuildmat.2022.128447
50. Kadapure, S.A.; Deshannavar, U.B. (Bio-smart material in self-healing of concrete. *Materials Today: Proceedings* **2022**, *49*, 1498–1503. https://doi.org/10.1016/j.matpr.2021.07.245
51. Phillips, A.J.; Gerlach, R.; Lauchnor, E.; Mitchell, A.C.; Cunningham, A.B.; Spangler, L. Engineered applications of ureolytic biomineralization: a review. *Biofouling* **2013**, *29*, 715–733. https://doi.org/10.1080/08927014.2013.796550
52. Gao, Y.; Zhu, X.; Corr, D.J.; Konsta-Gdoutos, M.S.; Shah, S.P. Characterization of the interfacial transition zone of CNF-Reinforced cementitious composites. *Cem. Concr. Compos.* **2019**, *99*, 130–139. https://doi.org/10.1016/j.cemconcomp.2019.03.002